

Experimental and kinetic simulation study of electron power absorption mode transitions in capacitive radiofrequency discharges in neon

B Horváth^{1,5} , A Derzsi^{1,2} , J Schulze^{2,3,4} , I Korolov³ , P Hartmann¹  and Z Donkó¹ 

¹ Institute for Solid State Physics and Optics, Wigner Research Centre for Physics, 1121 Budapest, Hungary

² Department of Physics, West Virginia University, Morgantown, WV 26506, United States of America

³ Institute of Electrical Engineering and Plasma Technology, Ruhr-University Bochum, 44780 Bochum, Germany

⁴ Key Laboratory of Materials Modification by Laser, Ion and Electron Beams, School of Physics, Dalian University of Technology, People's Republic of China

E-mail: horvath.benedek@wigner.hu

Received 29 November 2019, revised 18 February 2020

Accepted for publication 19 March 2020

Published 28 April 2020



Abstract

The spatio-temporal ionization and excitation dynamics in low-pressure radiofrequency (RF) discharges operated in neon are studied and a detailed comparison of experimental and kinetic simulation results is provided for a wide parameter regime. Phase resolved optical emission spectroscopy (PROES) measurements and 1d3v particle-in-cell/Monte Carlo collisions (PIC/MCC) simulations are performed in a geometrically symmetric capacitively coupled plasma (CCP) reactor at driving frequencies ranging from 3.39 MHz to 13.56 MHz, pressures between 60 Pa and 500 Pa, at a peak-to-peak voltage of 330 V. We examine the applicability of PROES (which provides information about the spatio-temporal distribution of the electron-impact excitation dynamics from the ground state into the Ne 2p₁ state) to probe the discharge operation mode in neon (which is determined by the spatio-temporal distribution of the ionization dynamics). We find that the spatio-temporal excitation rates measured by PROES are in a good agreement with the excitation rates obtained from the PIC/MCC simulations, for all the discharge conditions studied here. However, the ionization dynamics is found to be significantly different from the excitation dynamics under most of the discharge conditions studied here, especially at higher values of the driving frequency and lower values of the pressure, when energetic heavy particle induced secondary electrons (γ -electrons) are more likely to ionize than to excite. PROES does not probe the discharge operation mode under these conditions. At a fixed frequency and peak-to-peak voltage, the spatio-temporal distribution of the ionization rate obtained from PIC/MCC simulations shows a transition of the discharge operation mode from the α -mode to the γ -mode by increasing the pressure. However, PROES fails to show this transition. While in the spatio-temporal distribution of the excitation rate obtained from the PROES measurements and the PIC/MCC simulations the α -peak (the intensity maximum at the bulk side of the expanding sheath edge) is dominant and a γ -peak (a maximum near the edge of the fully expanded sheath) becomes visible only at high values of the pressure or at the lowest frequency of 3.39 MHz, a γ -peak is visible in the

⁵ Author to whom any correspondence should be addressed.

ionization rate for all operation conditions, and it dominates the ionization in the vast majority of the cases investigated.

Keywords: capacitively coupled plasma, electron power absorption, discharge operation mode, ionization dynamics, PIC/MCC simulation, phase resolved optical emission spectroscopy

(Some figures may appear in colour only in the online journal)

1. Introduction

Capacitively coupled plasmas (CCPs) have been widely studied in order to optimize their applications, such as etching and deposition [1–4]. In these applications, the interaction of the charged heavy particle species with the electrodes plays an important role. Since ions are mostly generated in electron-impact collisions within the plasma, understanding the electron power absorption mechanisms of RF discharges is essential and has been intensively studied [5–31]. Recently, the understanding of the effects of the various plasma-surface interactions on the discharge characteristics based on realistic models has also become a central issue [32–41].

The electron power absorption and ionization dynamics of CCPs determine the discharge operation mode. Low-pressure CCPs generated in electropositive gases have two characteristic operation modes in terms of the ionization dynamics: the α -mode and the γ -mode [5]. In the α -mode, the ionization is concentrated at the bulk side of the expanding sheath edge at both electrodes. During sheath expansion, electrons gain energy from the high electric field that accelerates them away from the electrodes, and these high-energy electrons cause intensive ionization [6–8, 10, 21]. In the γ -mode, however, the ionization is concentrated within the sheaths. In this case, secondary electrons (SEs) originating from the electrodes due to ion or neutral impact (γ -electrons) [42] play a dominant role in the ionization dynamics. The γ -electrons are accelerated by the high electric field within the sheaths, causing strong ionization at the times of high sheath voltage [5]. At higher pressures, the efficient collisional multiplication of the γ -electrons within the sheaths results in further enhancement of the γ -mode ionization. While in electropositive CCPs operated at low pressures or low driving voltages the α -mode ionization dynamics dominates in the discharge, the γ -mode ionization dynamics usually dominates in CCPs characterised by efficient secondary electron emission (SEE) from the (e.g. dielectric) electrode surfaces, at high pressures and/or high applied voltages. Under certain discharge conditions, other types of discharge operation modes can be found, e.g. the Ω -mode in atmospheric pressure plasmas (in which ionization in the bulk dominates) [19, 26], the drift–ambipolar (DA) mode in electronegative plasmas (in which drift and ambipolar electric fields accelerate the electrons, which cause significant ionization across the bulk and at the collapsing sheath edge) [18], and the striation mode in strongly electronegative plasmas (where the ion–ion plasma in the bulk region resonates with the excitation frequency) [22, 25, 31].

The discharge operation mode can be identified based on the spatio-temporal distribution of the ionization rate. Both experimental and computational methods have been developed for examining the operation modes of RF discharges. As an experimental method, phase resolved optical emission spectroscopy (PROES) is often applied. PROES is a powerful technique for the spatio-temporal observation of the optical emission of plasmas at specific wavelengths, based on which the excitation rate of a certain atomic state can be studied experimentally [13, 14, 43]. With the appropriate choice of an emission line resulting from electron-impact excitation with a high threshold energy, one can gain insight into the dynamics of high-energy electrons. As ionization, the fundamental process regarding the CCP discharge operation, is also caused by high-energy electrons, PROES is often applied to reveal the discharge operation mode. However, the spatio-temporal distributions of the excitation and the ionization rates can be remarkably different from each other [11]. They will only be similar, if (i) the threshold of the experimentally observed electron impact excitation into a specific level is close to the ionization threshold, and (ii) the cross sections of the excitation into the observed level and the ionization as a function of the electron energy have similar shapes within the energy range of electrons in the discharge. If any of these conditions is not fulfilled, the application of PROES to probe the ionization dynamics, i.e. the discharge operation mode of CCPs can be problematic.

The spatio-temporal distribution of the rates of the elementary collision processes, including ionization and excitation, can be obtained from computational approaches, like particle-in-cell/Monte Carlo collisions (PIC/MCC) simulations [44–54]. Since the cross section of electron impact ionization as a function of the electron energy typically has a different shape than the cross sections of the various excitation channels, the spatio-temporal distribution of the excitation observable by PROES is expected to show a different picture from the ionization dynamics. On the other hand, the comparison of the results for the spatio-temporal excitation rate obtained from PROES measurements and PIC/MCC simulations can be used as a validation for both methods. For example, γ -CAST, a computationally assisted spectroscopic technique for the estimation of the effective SEE coefficient, is based on this kind of comparison [55].

For several reasons to be discussed in section 2, the $2p_1$ state of neon is an appropriate excited level to be used for PROES. It is widely used for the spectroscopy of RF discharges operated in different gases and gas mixtures, by adding neon as a

trace gas to the background gas in a low concentration. Liu *et al* [56] have recently investigated mode transitions experimentally in asymmetric CCPs operated in pure neon, by measuring the electron density and the average emission intensity of discharges from the $2p_1$ excited state. They observed transitions from the α - to the γ -mode as the driving voltage was increased at fixed pressures and fixed driving frequencies. The mode transitions were identified via the different dependence of the electron density and the emission intensity (which is proportional to the excitation rate) on the driving voltage: while the emission intensity increased linearly, the plasma density increased exponentially because of the high number of ionizations above a critical voltage, which was identified as the transition point. An important finding of [56] was that this mode transition could not be observed via the emission intensity, since the cross section of ionization in neon had a different dependence on the electron energy than the cross section of Ne $2p_1$ excitation.

Although both PROES and PIC/MCC simulation are widely applied methods for studying the excitation and ionization dynamics of RF discharges, a systematic comparison of computational and experimental results focusing on the relation of the spatio-temporal distributions of the excitation and the ionization rate in neon CCPs operated in a wide parameter regime has not been performed yet. In this work, we present and discuss such a comparison. PROES measurements of the Ne $2p_1$ state are performed in a geometrically symmetric CCP reactor. The discharges are operated in pure neon, which allows a detailed comparison of the excitation and ionization dynamics obtained from experiments and simulations under exactly the same discharge conditions. This way the uncertainty resulting from the interaction of the trace gas with the discharge gas (usually neglected in the simulations) is excluded. Single-frequency neon discharges are studied here in a wide range of the driving frequency (from 3.39 MHz to 13.56 MHz) and the pressure (from 60 Pa to 500 Pa). The peak-to-peak voltage is kept constant at 330 V. This study reveals the dependence of the electron power absorption and ionization dynamics on these operation parameters. In addition, the applicability of PROES to probe the discharge operation mode is also examined in a wide parameter regime.

The paper is structured in the following way: in section 2, the experimental setup is described in detail, while in section 3, the simulation method is introduced. In section 4, the results are shown and discussed, and the conclusions are drawn in section 5.

2. Experimental setup and discharge conditions

For the experimental study of the space and time resolved optical emission of CCPs, PROES is used at a geometrically symmetric CCP source ('Budapest v.3'). A sketch of the experimental setup is shown in figure 1. The electrodes are located inside a quartz cylinder. The chamber can be evacuated when the gate valve is open, via a turbomolecular and a rotary pump. The base pressure of the system is approximately 10^{-5} Pa. The experiments are performed in a gas flow of ~ 3 sccm set by a flow controller. A needle valve allows fine control

of the gas pressure in the chamber. The stainless steel electrodes are plane-parallel and circular with identical diameters of 14.2 cm, while the gap between them is 2.5 cm. The upper electrode is driven by an RF waveform generator (Juntek JDS-2900), to which it is connected via a linear power amplifier (RM BLA-300) and an impedance matching box (MFJ-949E) that can be tuned for different values of the driving frequency, in order to maximize the power delivered to the plasma. The lower electrode is grounded. The voltage between the electrodes is monitored by a high voltage probe (HP 10076A, 100:1), and the pressure can be measured by a capacitive gauge (MKS 631A11MDEH, type 631).

The main diagnostic tool of the setup is a fast-gateable ICCD camera (4 Picos, Stanford Computer Optics), by which the emission from the Ne $2p_1$ state at a wavelength of 585.25 nm is measured space and time resolved. The camera is equipped with an interference filter with a central wavelength of 585 nm and a spectral full width at half maximum of 10 nm. The trigger signal of the camera is synchronized with the waveform generator. The gatewidth of the camera varies from 2 ns to 4 ns in the current study, while the length of the RF period varies between 73.7 ns (13.56 MHz) and 295.0 ns (3.39 MHz). The spatial resolution is determined by the number of pixels in the camera sensor: the 170 pixels result in a resolution of approximately $150\ \mu\text{m}$. The camera has a telecentric lens (Thorlabs MVTC23013 0.128x bi-telecentric lens), by which two-dimensional pictures can be taken. Due to the lateral uniformity of the plasma, the data are averaged in the direction perpendicular to the discharge axis, which reduces the noise significantly.

The theoretical consideration behind PROES is based on population dynamics: the method operates based on the time-dependent measurement of the population density of a specifically chosen excited rare gas state, as introduced in [14]. The basic concept of the measurement is that the spatio-temporal electron impact excitation rate from the ground state into the observed level, $E_{0,i}(x, t)$, can be calculated from the measured spatio-temporal emission. In order to perform a PROES measurement on a CCP based on the analysis presented in [14], several conditions need to be satisfied [14]:

- (a) The relevant optical transition rates need to be known.
- (b) The population of the excited states due to cascades, excitation from metastable levels and quenching need to be negligibly low.
- (c) Enough intensity of the measured emission line is necessary and superposition with other lines within the spectral resolution of the spectrometer or the interference filter has to be avoided.
- (d) The lifetime of the relevant excited state has to be short enough to temporally resolve the RF period (the shortest period being ~ 74 ns here).

One transition that satisfies these criteria well in neon gas is the emission line at 585.25 nm originating from the Ne $2p_1$ state with a lifetime of 16.26 ns and a threshold energy for electron impact excitation from the ground state of 18.965 eV [57].

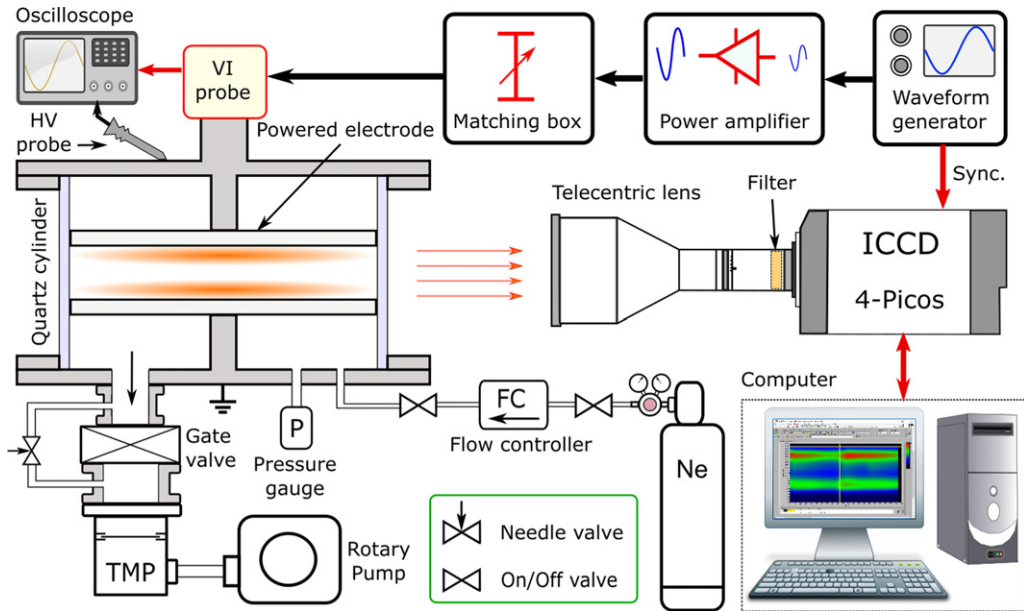


Figure 1. Scheme of the experimental setup.

Within the frame of this work, the discharge conditions are varied as follows: the driving frequency ranges from 3.39 MHz to 13.56 MHz, the pressure is set between 60 Pa and 500 Pa, while the peak-to-peak voltage is fixed at 330 V.

3. Simulation method

Particle-in-cell/Monte Carlo collisions (PIC/MCC) simulations [44–54] are widely used to study the electron power absorption and ionization dynamics of low-pressure CCPs. The PIC method has two crucial assumptions: (i) instead of tracing individual particles, superparticles are traced, which represent a large number of real particles, and (ii) instead of considering the pairwise interactions of the charged particles, a meanfield approximation is used for the calculation of the electrostatic interactions. These assumptions are complemented with a Monte Carlo type modelling of the particle collisions, i.e. the occurrence of elementary processes is determined according to their cross sections, with the use of random numbers. The PIC/MCC simulation code used in this work is one dimensional in space and three dimensional in velocity space (1d3v), which is suitable to describe CCPs with planar electrodes of identical surface areas.

In our PIC/MCC simulations of RF discharges in neon, the particles traced are Ne^+ ions and electrons. The cross sections of the collision processes are shown in figure 2. For the collision of electrons with Ne atoms, elastic scattering, excitation and ionization are considered, and their cross sections are taken from the Biagi-v7.1 dataset [58]. Nine possible atomic excitation processes are taken into account (shown as solid lines in figure 2). One of them is the $\text{Ne} 2p_1$ excitation process from the ground state (shown by the thick continuous line), i.e. the state whose population dynamics is observed experimentally by PROES. For the collision of Ne^+ ions with Ne atoms, isotropic and backward elastic scattering is considered [59].

The surface processes taken into account are electron reflection and SEE induced by ions. Both are described in a simplified way in the present PIC/MCC simulations, i.e. constant surface coefficients are specified for these processes. In case of the electrons hitting the electrode surface, a constant probability of $\eta_e = 0.2$ is assumed for elastic electron reflection [60]. Although a realistic treatment of the interaction of electrons with the electrodes should consider energy-dependent coefficients for elastic electron reflection [61, 62], such a realistic treatment of electron reflection is not expected to cause a remarkable difference regarding the spatio-temporal distribution of the excitation and the ionization rate at the relatively high pressures considered here. At low electron energies (below 10 eV) a realistic electron reflection coefficient can be higher than 0.2 for some surface materials. A change of the electron reflection probability at the electrodes causes a change of the plasma density and the ion flux to the electrodes, but this will affect the α - and γ -maximum of the excitation and the ionization in a similar way, since the maximum of sheath expansion is sensitive to the electron density and the maximum due to SEEs depends on the ion flux to the electrodes. Daksha *et al* [55] studied the effect of changing this reflection probability on the ratio of the intensities of both maxima and found it to remain approximately constant. This means that the mode of discharge operation is insensitive to this parameter. For the treatment of the interaction of Ne^+ ions with the electrodes, a constant SEE coefficient of $\gamma = 0.29$ is used in most of the simulations in this work, which was determined by γ -CAST [55], as it will be described later. In addition, some calculations are performed with other γ values, in order to demonstrate the effects of ion-induced SEEs (γ -electrons) on the discharge characteristics. In fact, not only ions can cause the emission of electrons from the electrodes. Other particles like photons and metastables can also contribute to the SEE [42]. The assumption of a γ -coefficient for the ions hitting

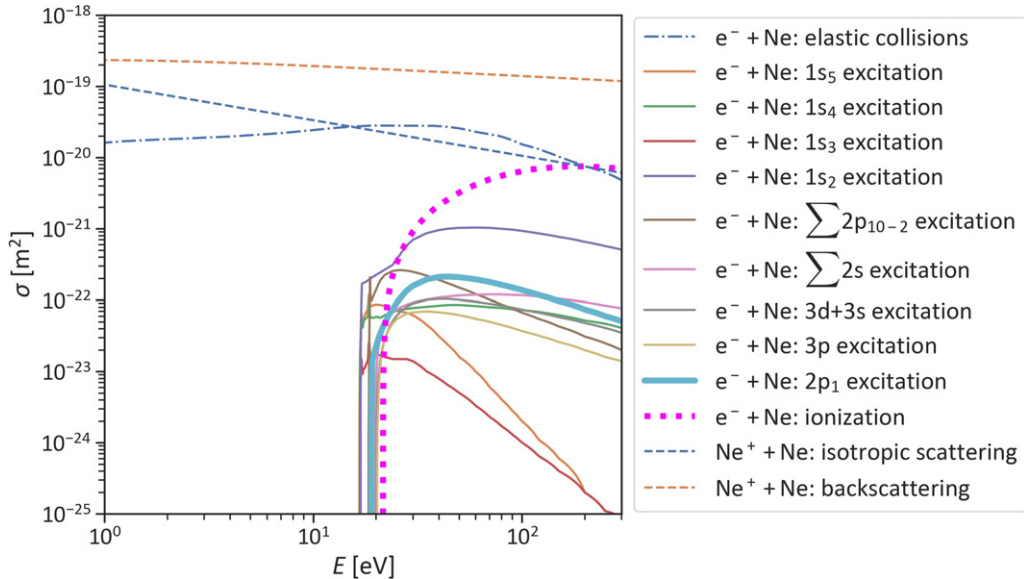


Figure 2. Cross sections of the collision processes considered in the PIC/MCC simulations of neon CCPs, as a function of the kinetic energy of the projectile. For ions, E is the kinetic energy in the center-of-mass frame. The dash-dot line corresponds to the electron–atom elastic scattering, while the thin solid lines correspond to the electron–atom excitation channels. The thick solid line represents the $\text{Ne } 2\text{p}_1$ electron-impact excitation from the ground state, and the thick dotted line corresponds to electron-impact ionization. The dashed lines correspond to ion-atom isotropic elastic scattering and elastic backscattering, respectively.

the electrode surface implicitly considers all these different kinds of energy-dependent processes in a simplified way, i.e. an effective γ -coefficient is used in the simulations [32].

The simulation results for the spatio-temporal distributions of the ionization and the excitation rates are compared to those of the measured excitation. In the simulations, the elementary excitation and ionization collisions are counted in a space and time dependent way within several thousands of RF cycles, and the results are averaged. The position of the sheath edge relative to the respective electrode, $s(t)$ is calculated by a criterion proposed in [63]:

$$\int_0^{s(t)} n_e(x', t) dx' = \int_{s(t)}^{L/2} (n_i(x', t) - n_e(x', t)) dx', \quad (1)$$

where x' is the position relative to the respective electrode within the electrode gap, L is the length of the electrode gap, n_e and n_i are the electron and ion densities.

4. Results and discussion

In this section, the results of the PROES measurements and the PIC/MCC simulations are presented and compared for a wide parameter regime. Both in the simulations and the experiments, the neon gas pressure ranges from 60 Pa to 500 Pa and the frequency of the driving voltage is varied between 3.39 MHz and 13.56 MHz. The peak-to-peak value of the driving voltage, V_{pp} , is set to 330 V and the electrode gap is $L = 2.5$ cm. At first, the influence of the γ SEE coefficient on the calculated discharge characteristics is demonstrated in section 4.1, and the determination of the γ -coefficient used in the current study is introduced. In section 4.2, the effect of

varying the pressure is studied at different driving frequencies, and a systematic comparison of PROES measurement and PIC/MCC simulation results for the excitation and the ionization dynamics is presented.

4.1. Effect of the γ -coefficient

In PIC/MCC simulations of RF discharges, the choice of the γ SEE coefficient is crucial, especially at high pressures and low frequencies, when γ -electrons can be efficiently multiplied within the sheaths. An unrealistic γ -coefficient can underestimate or overestimate the ionization caused by SEEs in the discharge, causing unrealistic results for the plasma density and other plasma parameters.

In figure 3, the influence of the γ -coefficient on the spatio-temporal distribution of the excitation and the ionization rates is demonstrated: PIC/MCC simulation results obtained by assuming different values for the γ SEE coefficient are presented and compared to the PROES result for a driving frequency of 6.78 MHz, a peak-to-peak voltage of 330 V and a pressure of 500 Pa. Simulation results with γ coefficients of 0.2 [panels (a) and (e)], 0.29 [panels (b) and (f)] and 0.35 [panels (c) and (g)] are shown in the first three rows, while the experimental result on the $\text{Ne } 2\text{p}_1$ excitation rate obtained from PROES is shown in panel (d). In each panel, the horizontal axis corresponds to one RF period, and the vertical axis shows the distance from the powered electrode, i.e. $x/L = 0$ is the position of the powered electrode and $x/L = 1$ is the position of the grounded one. In case of $\gamma = 0.2$, the excitation is concentrated near the sheath edges (figure 3(a)), i.e. a strong α -peak can be seen. As the SEE coefficient is increased to 0.29, the excitation becomes significant within the sheaths, while it is still strong at the sheath edges (figure 3(b)). The α -peak has

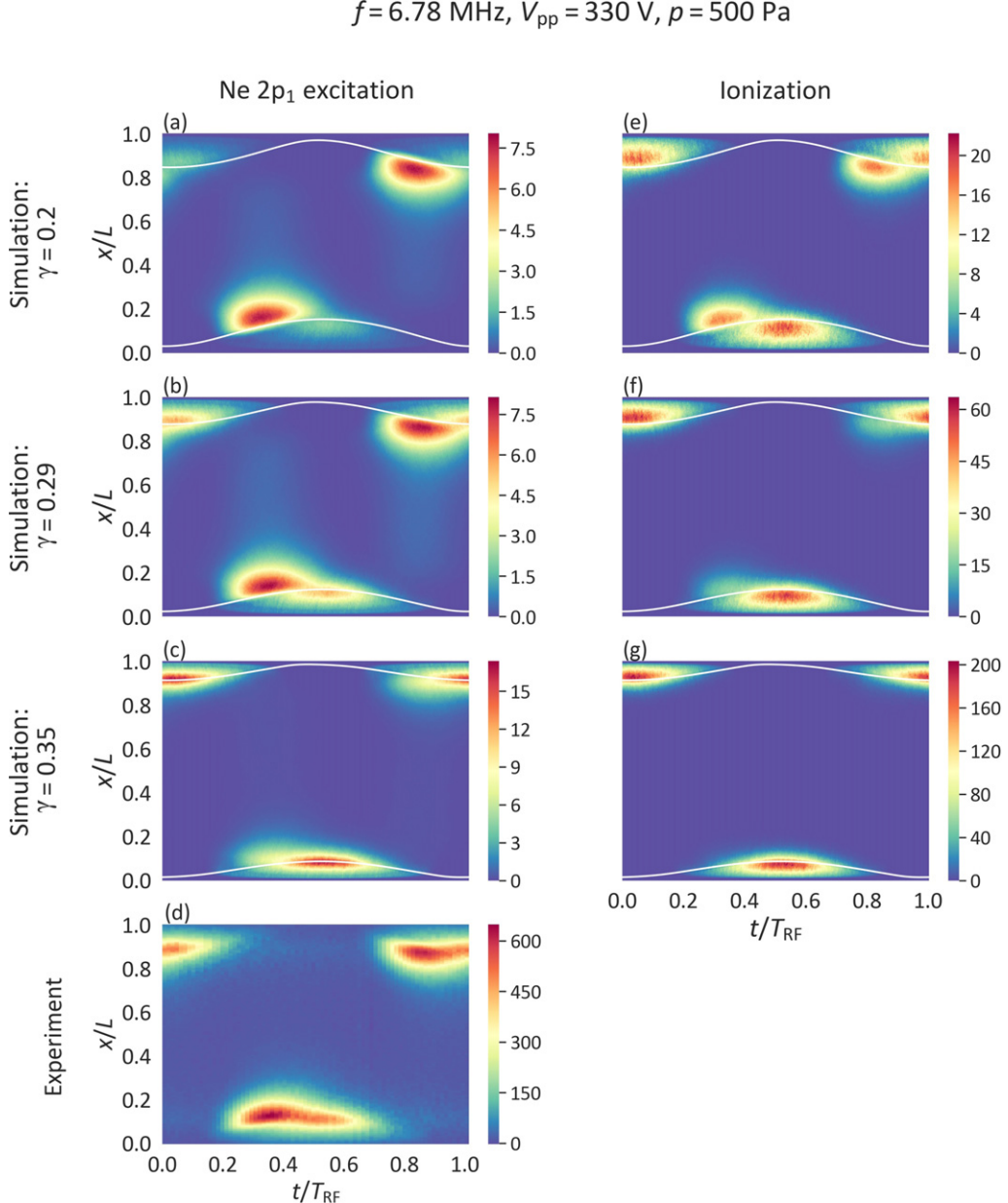


Figure 3. Spatio-temporal plots of the electron-impact excitation rate from the ground state into the Ne 2p₁ state obtained from PIC/MCC simulations [$10^{20} \text{ m}^{-3} \text{ s}^{-1}$] (a)–(c) and measured by PROES [a.u.] (d), as well as the ionization rate obtained from PIC/MCC simulations [$10^{21} \text{ m}^{-3} \text{ s}^{-1}$] (e)–(g). In the simulations, different coefficients for the ion-induced secondary electron emission are considered: $\gamma = 0.2$ (1st row), 0.29 (2nd row) and 0.35 (3rd row). The sheath edges obtained from the simulations are shown as white lines. The powered electrode is located at $x/L = 0$, while the grounded electrode is at $x/L = 1$. Discharge conditions: $f = 6.78 \text{ MHz}$, $L = 2.5 \text{ cm}$, $V_{\text{pp}} = 330 \text{ V}$, $p = 500 \text{ Pa}$. $T_{\text{RF}} = 1/f$.

higher average intensity than the γ -peak under these conditions. In case of $\gamma = 0.35$, the excitation is dominant within the sheaths, being negligible at the sheath edges (figure 3(c)), i.e. a strong γ -peak can be seen. Based on the spatio-temporal plot of the excitation rate obtained from the PROES measurement (figure 3(d)), it is high both at the sheath edges and within the sheaths, the α -peak being stronger. Meanwhile, by increasing the value of the SEE coefficient, a transition of the discharge operation mode can be observed in the ionization dynamics (figures 3(e)–(g)): at $\gamma = 0.2$, the spatio-temporal distribution of the ionization rate exhibits a hybrid α – γ -mode (figure 3(e)), while for the largest value of $\gamma = 0.35$, a pure γ -mode can be

observed (figure 3(g)). These results show that the value of γ is absolutely critical in terms of the discharge operation mode. We note that the ionization dynamics is significantly different from the excitation dynamics for all values of γ under these conditions.

A comparison of the excitation rates obtained from PIC/MCC simulations for different values of γ to the PROES result for the same discharge conditions reveals that using $\gamma = 0.2$ in the simulation underestimates, while using $\gamma = 0.35$ overestimates the role of SEE in the discharge. On the other hand, an intermediate value of $\gamma = 0.29$ results in a good agreement between the PIC/MCC simulation and the PROES

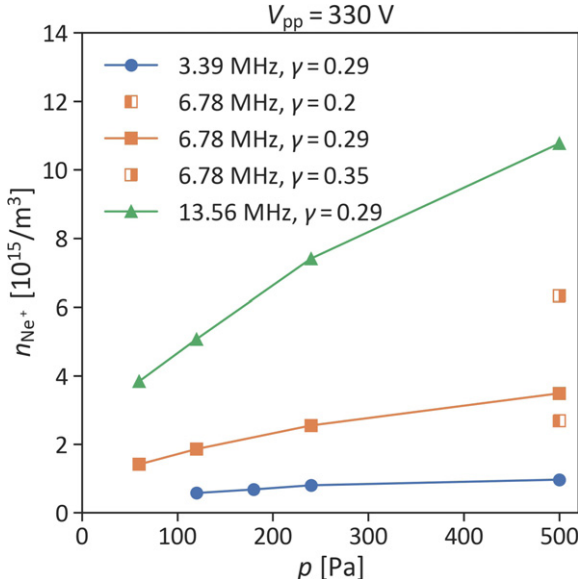


Figure 4. PIC/MCC simulation results: peak ion density as a function of pressure, for different values of the driving frequency and the γ SEE coefficient. Discharge conditions: $L = 2.5$ cm, $V_{pp} = 330$ V.

measurement for the excitation rate [figure 3(b) compared to figure 3(d)].

In figure 4, the peak ion densities obtained from the PIC/MCC simulations are shown as a function of the pressure, at a peak-to-peak voltage of 330 V and driving frequencies of 3.39 MHz, 6.78 MHz and 13.56 MHz. The effect of changing the SEE coefficient on the calculated ion density is shown for 6.78 MHz, by varying γ between 0.2 and 0.35 at 500 Pa. At a fixed frequency, the peak ion density increases as a function of the pressure. At a fixed pressure, the peak ion density also increases as the driving frequency is increased, and this difference in the density between the discharges operated at different driving frequencies is more pronounced at higher pressures. The choice of the SEE coefficient, γ , is also critical in terms of the ion density. At 6.78 MHz and 500 Pa, the density increases by a factor of ~ 2.6 as the SEE coefficient is changed from 0.2 to 0.35.

In order to determine a value for γ that is reliable for the discharge conditions studied in this work, the γ -CAST method is used [55], which is nothing else but a quantitative implementation of searching for the best match between the $\text{Ne } 2\text{p}_1$ excitation rates obtained by PROES and the corresponding excitation rates obtained by PIC/MCC simulations, by varying the SEE coefficient. This study is carried out for a pressure of 500 Pa, peak-to-peak voltage of 330 V, and driving frequencies of 3.39 MHz and 6.78 MHz, assuming various values for the γ -coefficient between 0.2 and 0.35 (results for selected values of γ are shown in figure 3 for 6.78 MHz). The reason why γ -CAST is done for these discharge parameters is that SEs have the most significant impact on the discharge under these conditions. As a first step of the γ -CAST, the average intensities of the α -peak (the excitation maxima at the bulk side of the sheath edge), I_α and the γ -peak (the excitation maxima near the edge of the fully expanded sheath), I_γ are calculated for the Ne

2p_1 excitation rates obtained from PROES measurement and PIC/MCC simulations. For a certain intensity peak, a region of interest (ROI) is defined as a rectangle in which the intensity is higher than 80% of the local maxima, and the intensity is averaged over it [55]. After that the I_γ/I_α ratios of the peaks are compared for the measurement and the PIC/MCC simulations. In the case of 3.39 MHz, 500 Pa and 330 V, the best agreement between the simulation and the experiment was found between $0.280 < \gamma < 0.290$, while for 6.78 MHz, it was found for $0.295 < \gamma < 0.300$. Based on that, $\gamma = 0.29$ was chosen to be used in all the following simulations for all discharge conditions. In reality, the value of the γ -coefficient depends on all the discharge conditions (e.g. driving voltage shape and amplitude, driving frequency, gas pressure, electrode gap distance), since the value of the ion-induced SEE coefficient (and the coefficients for SEE by other species that are all included in the effective γ -coefficient) depends on the incident particle energy [42], which is affected by these conditions. However, the use of the γ -coefficient of 0.29 for all the discharge conditions is not a rough simplification. The difference between the γ values obtained for different driving frequencies is minor (between 3% and 4% for 3.39 MHz and 6.78 MHz), and SEs are only critical in terms of influencing the discharge operation mode at higher values of the gas pressure, when the γ -electrons emitted from the electrode are efficiently multiplied within the sheaths.

4.2. Effect of the gas pressure

In this section, the effect of changing the pressure on the excitation and ionization dynamics is examined at different driving frequencies. From now on, $\gamma = 0.29$ is used in all simulations. In figures 5–7, the spatio-temporal plots of the $\text{Ne } 2\text{p}_1$ excitation rate obtained by PROES measurements and PIC/MCC simulation results for the excitation rate and for the ionization rate are compared.

The highest frequency studied in this work is 13.56 MHz, for which the results are shown in figure 5. The peak-to-peak voltage is fixed at 330 V, while the effect of changing the pressure is examined between 60 Pa and 500 Pa. The rows of the figure from top to bottom correspond to different values of the gas pressure in increasing order. The columns from left to right correspond to the measured and computed excitation rate and the computed ionization rate, respectively. At this relatively high frequency, the spatio-temporal distributions of the $\text{Ne } 2\text{p}_1$ excitation rate obtained from PROES measurements (first column) and PIC/MCC simulations (second column) are in a very good agreement for all values of the pressure between 60 Pa and 500 Pa. In addition, the maximum sheath lengths obtained by PIC/MCC simulations are also very close to the ones observed in PROES measurements (in case of the PROES measurements, the sheath lengths are only visually estimated based on the excitation plot). On the other hand, the spatio-temporal distributions of the ionization rates obtained from PIC/MCC simulations are different from the excitation rates (see the third column compared to the first two). While both the experiment and the simulation show the excitation to be localized at the edge of the expanding sheaths

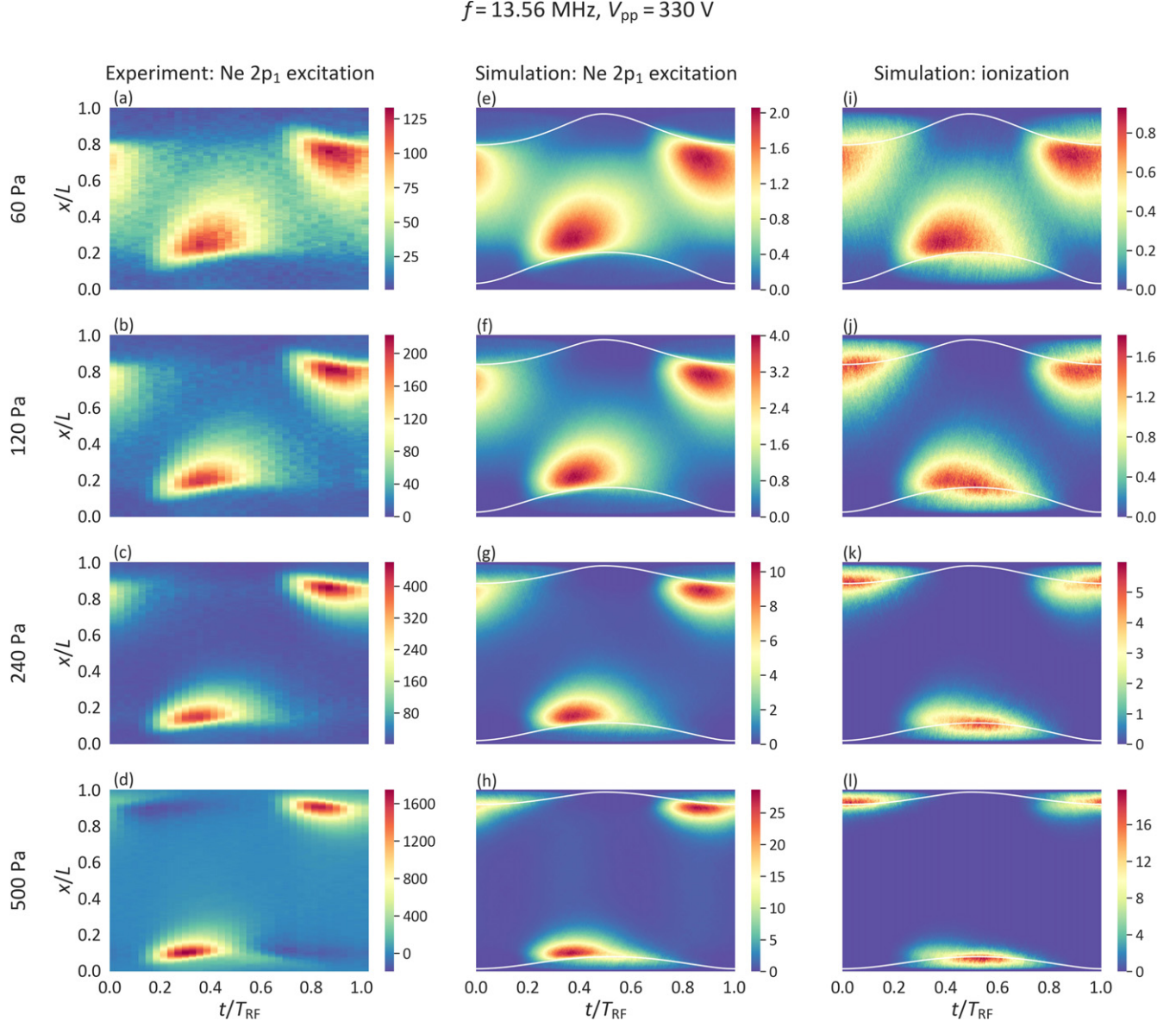


Figure 5. Spatio-temporal plots of the electron-impact excitation rate from the ground state into the Ne 2p₁ state measured by PROES [a.u.] (a)–(d) and obtained from PIC/MCC simulations [$10^{20} \text{ m}^{-3} \text{s}^{-1}$] (e)–(h), as well as the ionization rate obtained from PIC/MCC simulations [$10^{21} \text{ m}^{-3} \text{s}^{-1}$] (i)–(l) at different neutral gas pressures. The sheath edges obtained from the simulations are shown as white lines in panels (e)–(l). The powered electrode is located at $x/L = 0$, while the grounded electrode is at $x/L = 1$. Discharge conditions: $f = 13.56 \text{ MHz}$, $L = 2.5 \text{ cm}$, $V_{\text{pp}} = 330 \text{ V}$, the pressure is varied between 60 Pa and 500 Pa. $T_{\text{RF}} = 1/f$. $\gamma = 0.29$ is used in the simulations.

within the whole pressure range, which implies α -mode discharge operation, ionization can also be observed within the sheaths at a different time within the RF period. Although the α -mode ionization is dominant at 60 Pa, the discharge operation changes to pure γ -mode as the pressure is increased to 500 Pa [see figures 5(i)–(l)]. However, this transition cannot be observed in the spatio-temporal distribution of the excitation. At higher values of the pressure, the excitation clearly does not probe the ionization, i.e. the discharge operation mode cannot be observed by PROES under these conditions. The reason why the spatio-temporal distribution of the Ne 2p₁ excitation does not probe the ionization is the difference in the respective cross sections (see the thick solid and dotted lines in figure 2). Although their thresholds are close to each other (18.965 eV

for the excitation and 22 eV for the ionization), their shapes are different within the energy regime up to hundreds of eV, i.e. the energy regime of electrons in the discharge: while the cross section of excitation decreases above ~ 40 eV, the one of ionization continuously increases up to about 300 eV. This relation of the two cross sections causes that the ionization dynamics is more sensitive to high-energy electrons, i.e. significantly more ionization processes caused by energetic γ -electrons take place within the expanded sheaths than Ne 2p₁ excitation.

Figure 6 shows results for 6.78 MHz driving frequency. The value of the peak-to-peak voltage is again fixed at 330 V, while the pressure is varied between 60 Pa and 500 Pa, similarly to the case of 13.56 MHz (figure 5). For all values

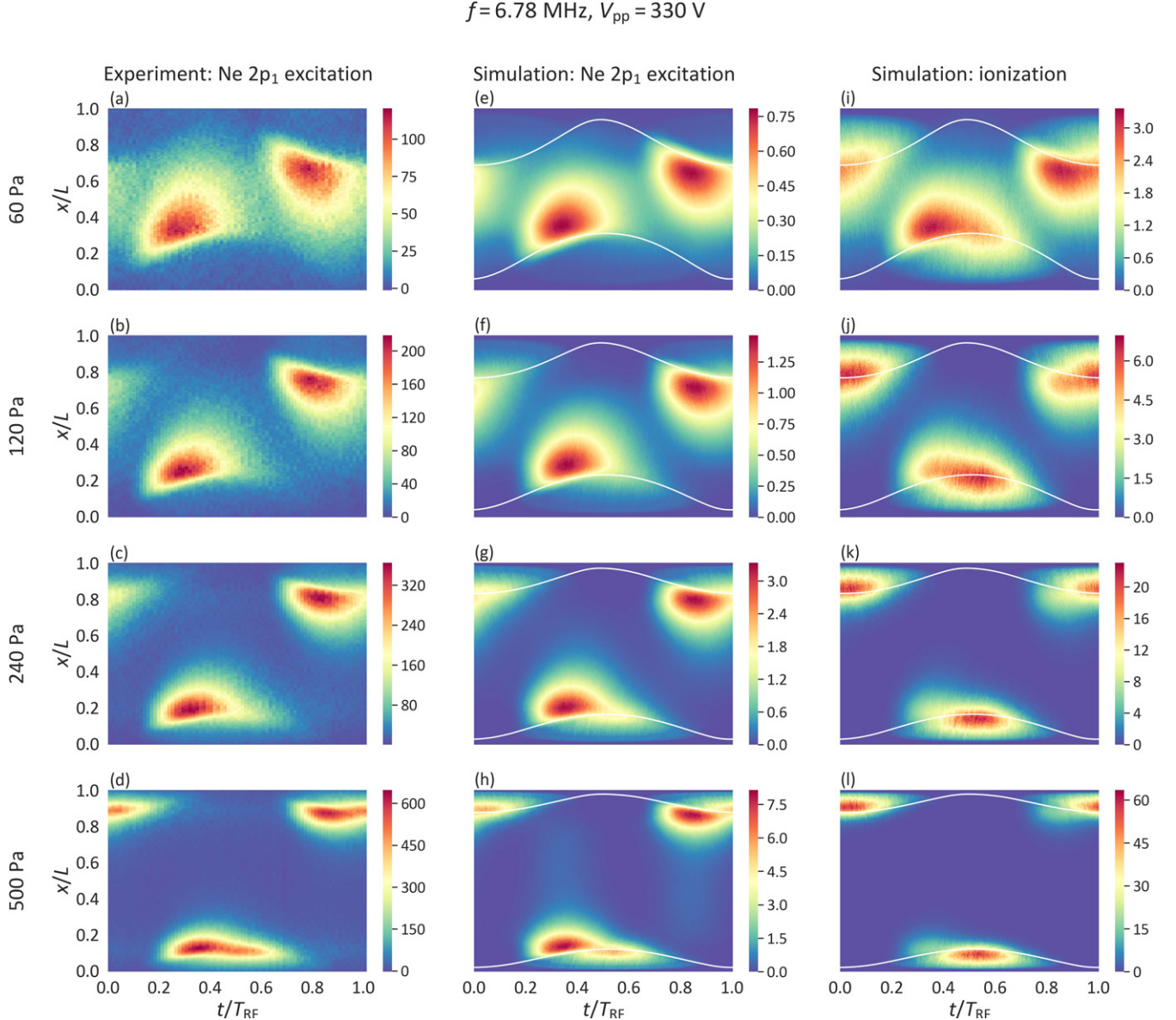


Figure 6. Spatio-temporal plots of the electron-impact excitation rate from the ground state into the Ne 2p₁ state measured by PROES [a.u.] (a)–(d) and obtained from PIC/MCC simulations [$10^{20} \text{ m}^{-3} \text{s}^{-1}$] (e)–(h), as well as the ionization rate obtained from PIC/MCC simulations [$10^{20} \text{ m}^{-3} \text{s}^{-1}$] (i)–(l) at different neutral gas pressures. The sheath edges obtained from the simulations are shown as white lines in panels (e)–(l). The powered electrode is located at $x/L = 0$, while the grounded electrode is at $x/L = 1$. Discharge conditions: $f = 6.78 \text{ MHz}$, $L = 2.5 \text{ cm}$, $V_{\text{pp}} = 330 \text{ V}$, the pressure is varied between 60 Pa and 500 Pa. $T_{\text{RF}} = 1/f$. $\gamma = 0.29$ is used in the simulations.

of the pressure, the excitation rates obtained from experiment and simulation are in a good agreement [see figures 6(a)–(d) in comparison with figures 6(e)–(h)]. Both in the simulations and the experiments, strong excitation peaks can be observed at the expanding sheath edges. The sheath lengths decrease as the pressure is increased, and the excitation inside the sheaths increases (see for example in figure 6(d) around $t/T_{\text{RF}} = 0.5$, at the powered electrode). At the highest pressure of 500 Pa, both the PROES measurement and the PIC/MCC simulation show strong excitation inside the sheaths (figures 6(d) and (h)): the excitation dynamics is significantly different from the case of 240 Pa (figures 6(c) and (g)) and lower pressures. Regarding the ionization rates obtained from PIC/MCC simulations (third column), a γ -peak in the sheaths is visible for all values

of the pressure. This γ -peak gets significantly stronger as the pressure is increased from 60 Pa to 500 Pa (figures 6(i)–(l)), i.e. a transition from dominant α -mode to pure γ -mode can be observed due to the enhanced collisional multiplication of SEs inside the sheaths at higher pressures. For all values of the pressure, the spatio-temporal distribution of the ionization rate significantly differs from the excitation rate: the ionization tends to be concentrated within the sheaths (γ -mode) for the pressures of 120 Pa and above, while the excitation mostly takes place at the sheath edges, which suggests α -mode. At higher values of the pressure, the PROES measurement clearly does not probe the ionization dynamics correctly. The reason is again the different shapes of the cross sections of the ionization and the Ne 2p₁ excitation: the relative probability of

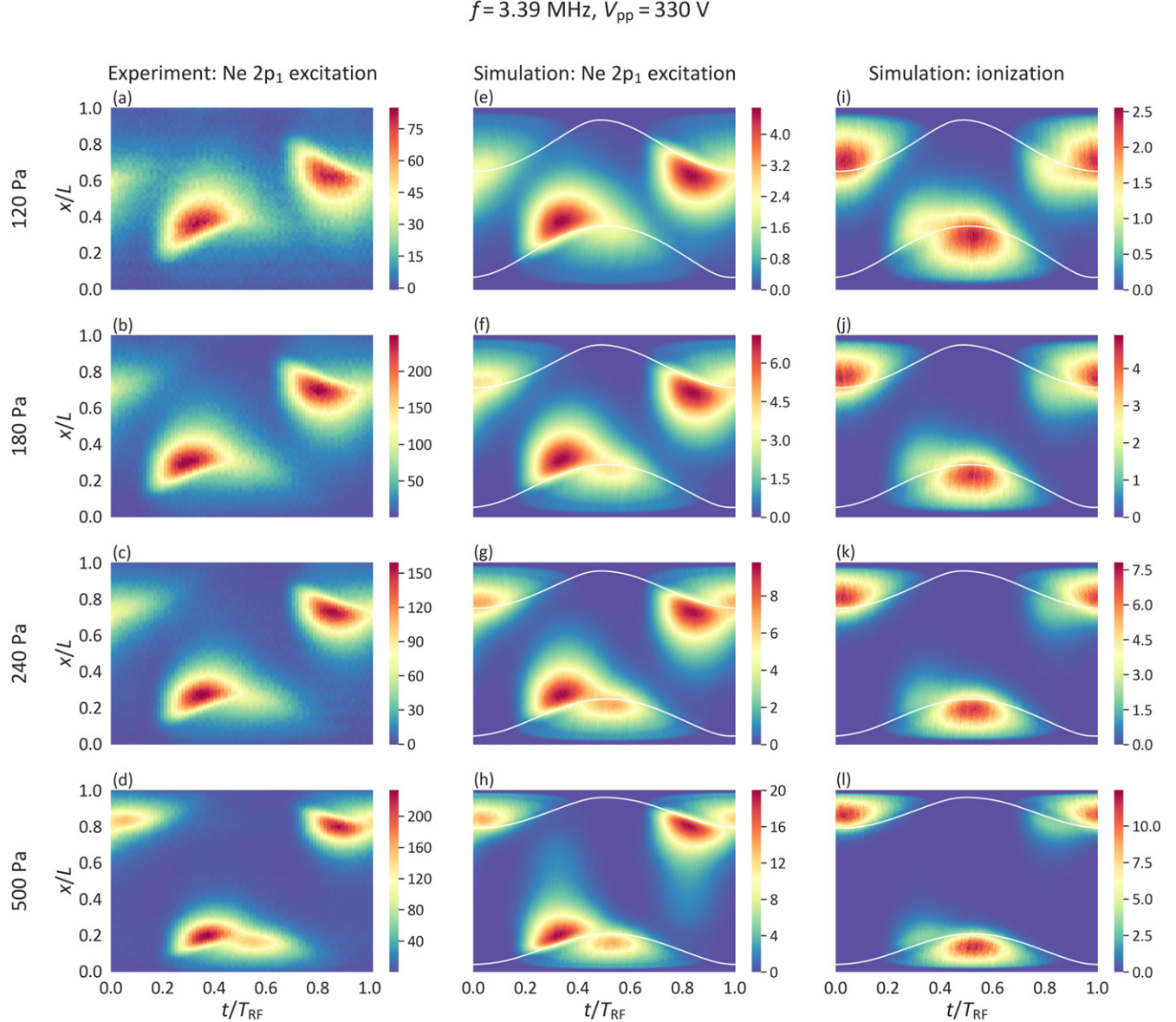


Figure 7. Spatio-temporal plots of the electron-impact excitation rate from the ground state into the Ne 2p₁ state measured by PROES [a.u.] (a)–(d) and obtained from PIC/MCC simulations [$10^{19} \text{ m}^{-3} \text{ s}^{-1}$] (e)–(h), as well as the ionization rate obtained from PIC/MCC simulations [$10^{20} \text{ m}^{-3} \text{ s}^{-1}$] (i)–(l) at different neutral gas pressures. The sheath edges obtained from the simulations are shown as white lines in panels (e)–(l). The powered electrode is located at $x/L = 0$, while the grounded electrode is at $x/L = 1$. Discharge conditions: $f = 3.39 \text{ MHz}$, $L = 2.5 \text{ cm}$, $V_{\text{pp}} = 330 \text{ V}$, the pressure varied between 120 Pa and 500 Pa. $T_{\text{RF}} = 1/f$. $\gamma = 0.29$ is used in the simulations.

ionization compared to Ne 2p₁ excitation increases with the electron energy, i.e. the highly energetic γ -electrons within the sheaths are more likely to ionize than to excite.

At the lowest frequency of 3.39 MHz studied in this work, the effect of changing the pressure on the discharge characteristics is examined between 120 Pa and 500 Pa, corresponding to the rows from top to bottom in figure 7. The reason why no results are shown for 60 Pa (as in the case of figure 5 and figure 6, corresponding to 13.56 MHz and 6.78 MHz) is that the discharge could not be maintained at such a low pressure at this low frequency. The Ne 2p₁ excitation rates measured by PROES (first column) and obtained from PIC/MCC simulations (second column) are again in a good agreement at this low frequency, however, the simulations show slightly stronger

excitation within the sheaths than the PROES measurements for all values of the pressure. This could be caused by a small variation of γ as a function of the driving frequency due to e.g. frequency-dependent changes of heavy particle energies at the electrodes. Such a variation of γ is not included in the simulations. Both in the simulations and the experiments, the excitation rates are high at the expanding sheath edge, and there is a γ -peak within the sheaths at the times of maximal sheath voltage, which intensifies as the pressure is increased from 120 Pa to 500 Pa. At 500 Pa, the measured and the simulated excitation rates [see figures 7(d) and (h)] suggest hybrid $\alpha-\gamma$ -mode, in which the α -peak is stronger.

In addition, the PIC/MCC simulation shows weak excitation inside the bulk plasma upon high magnitude of the

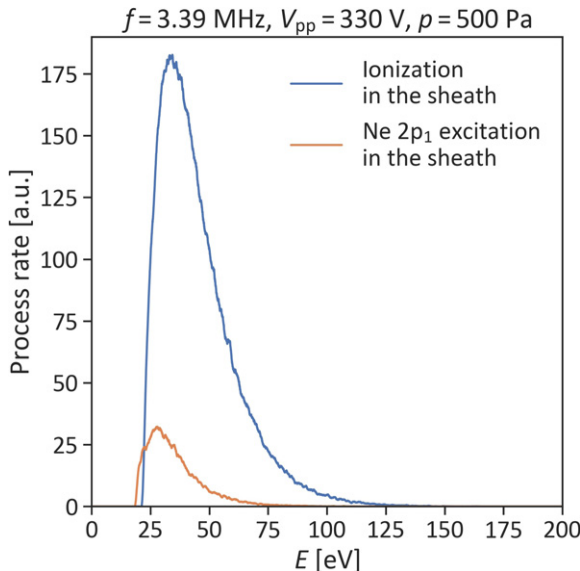


Figure 8. PIC/MCC simulation result: the energy-resolved ionization and Ne 2p₁ excitation rates caused by the electrons within a region inside the sheaths (see text). Discharge conditions: $f = 3.39$ MHz, $V_{pp} = 330$ V, $p = 500$ Pa, $L = 2.5$ cm, $\gamma = 0.29$.

applied voltage within the RF period at this high pressure, which indicates the development of a high electric field in that region and a trend towards the drift–ambipolar (DA) electron power absorption mode with increasing pressure (figure 7(h)). A weak excitation caused by the drift electric field can also be observed at higher frequencies at 500 Pa (figures 5(h) and 6(h)). No such excitation pattern is visible at lower pressures. The DA-mode is, however, not yet established at the pressures covered here, and ionization in the bulk cannot be observed, since the drift field and, thus, the electron energy is still relatively low, and the cross section of the ionization has a higher threshold energy than the Ne 2p₁ excitation.

In the ionization rates at the driving frequency of 3.39 MHz (figure 7, third column), dominant γ -mode operation can be observed by the PIC/MCC simulation for all pressures, and the minor ionization at the sheath edges decreases with increasing pressure (figures 7(i)–(l)). The observation of the Ne 2p₁ excited state by PROES does not reflect the ionization dynamics and the discharge operation mode correctly at any values of the gas pressure, as the excitation (obtained from experiment and simulation) and the ionization exhibit completely different spatio-temporal distributions. The reason for this difference can be explained by examining the energy-resolved ionization and Ne 2p₁ excitation rates caused by the electrons within the expanded sheath, i.e. the number of elementary ionization and excitation processes caused by electrons falling into a given energy bin. These curves are shown in figure 8 for 500 Pa. Processes were counted within a ‘rectangular’ domain between $0.4 < t/T_{RF} < 0.6$ and $0 < x/L < s_{max}$, where s_{max} is the maximum sheath length at the powered electrode. It can be seen that the energy distribution of the ionizing electrons is much wider. While the number of excitations drops down to a negligible value above ~ 50 eV, the number of ionizations remains high at higher energies, approximately until ~ 100 eV in the current case. This is the direct consequence of the relation of

the cross sections of the two processes (see figure 2): the cross section of excitation decreases above ~ 40 eV, while the one of ionization continuously increases within the energy regime of electrons in the discharge.

5. Conclusions

Within the frame of this work, the electron power absorption modes of low-pressure RF discharges operated in neon gas were studied, and a detailed comparison of computational and experimental results was provided in a wide parameter regime. 1d3v particle-in-cell/Monte Carlo collisions (PIC/MCC) simulations and phase resolved optical emission spectroscopy (PROES) measurements were performed in a geometrically symmetric CCP reactor at driving frequencies ranging from 3.39 MHz to 13.56 MHz and pressures from 60 Pa to 500 Pa, at a fixed peak-to-peak voltage of 330 V. At first, the critical role of the SEE coefficient assumed in the PIC/MCC simulations was studied and the SEE coefficient of the system was determined by γ -CAST as $\gamma = 0.29$.

At fixed frequencies of 3.39 MHz, 6.78 MHz and 13.56 MHz, discharge operation mode transitions were observed by increasing the pressure. In all cases, the electron-impact excitation rates from the ground state into the Ne 2p₁ state obtained from PROES measurements and PIC/MCC simulations showed a good agreement. However, it was revealed that significant γ -mode ionization can take place in the discharge even in the cases when it is not seen in the spatio-temporal distribution of the Ne 2p₁ excitation, i.e. the excitation does not always probe the ionization (as it is typically assumed for PROES). In fact, the relation of the excitation rate into the observed level and the ionization rate depends on the relation of the respective cross sections. Although the threshold energy of the Ne 2p₁ excitation process is close to the one of ionization, the cross section of excitation decreases above ~ 40 eV, while the one of ionization continuously increases within the electron energy range of the discharges studied here, making the highly energetic γ -electrons within the sheaths more likely to ionize than to excite. Via the comparison of experimental and computational data within a wide parameter regime, this study also revealed the limitations of PROES to probe the discharge operation mode, which is determined by the ionization dynamics.

As a final remark, a general conclusion regarding the applicability of PROES in other gases to probe the ionization dynamics is drawn. Figure 9 shows the electron-impact cross sections of neon, argon and helium, for ionization and excitation of specific states corresponding to some standard PROES lines, as a function of the electron energy. The cross sections for argon and helium are taken from [64]. From these data we come to the conclusion that in none of these cases a good agreement between the excitation rate and the ionization rate can be guaranteed. Therefore, while PROES measurements clearly provide very important information about the charged particle dynamics in the discharge, one should generally be careful with predicting the operation mode of the discharge based on these data.

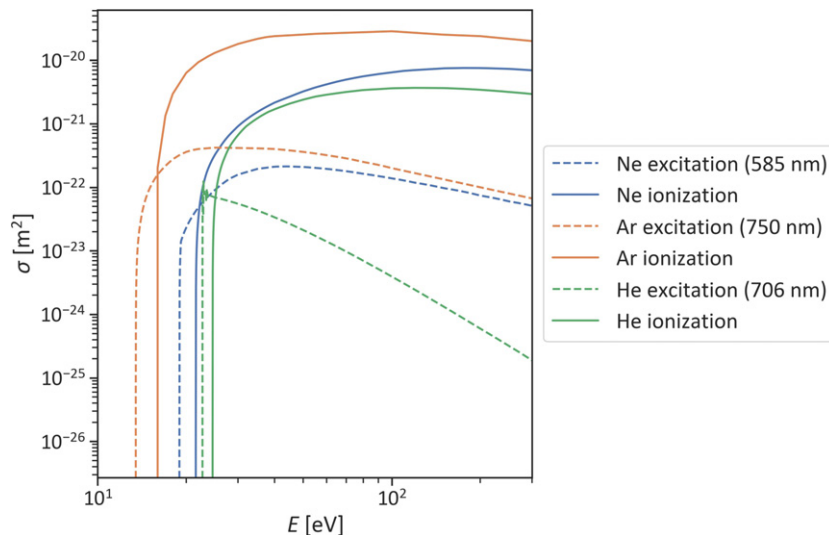


Figure 9. The electron-impact cross sections of neon, argon and helium for ionization and excitation from the ground state into specific excited states corresponding to standard PROES lines, as a function of the electron energy.

Acknowledgments

This work was supported by the Hungarian National Research, Development and Innovation Office via Grants K-119357, K-115805, PD-121033 and FK-128924, by the J Bolyai Research Fellowship of the Hungarian Academy of Sciences, by the ÚNKP-19-3 New National Excellence Program of the Ministry for Innovation and Technology, by the US NSF Grant No. PHY-1601080 and by the German Research Foundation (DFG) within the frame of the collaborative research centre SFB-TR 87 (project C1). We gratefully acknowledge the contribution of Mr Tibor Szűcs to the development of the experimental apparatus.

ORCID iDs

B Horváth <https://orcid.org/0000-0002-2371-2444>
A Derzsi <https://orcid.org/0000-0002-8005-5348>
J Schulze <https://orcid.org/0000-0001-7929-5734>
I Korolov <https://orcid.org/0000-0003-2384-1243>
P Hartmann <https://orcid.org/0000-0003-3572-1310>
Z Donkó <https://orcid.org/0000-0003-1369-6150>

References

- [1] Lieberman M A and Lichtenberg A J 2005 *Principles of Plasma Discharges and Materials Processing* 2nd ed (New York: Wiley)
- [2] Makabe T and Petrović Z 2006 *Plasma Electronics: Applications in Microelectronic Device Fabrication* (London: Taylor and Francis)
- [3] Chabert P and Braithwaite N 2011 *Physics of Radio-Frequency Plasmas* (Cambridge: Cambridge University Press)
- [4] Makabe T 2019 *Jpn. J. Appl. Phys.* **58** 110101
- [5] Belenguer P and Boeuf J P 1990 *Phys. Rev. A* **41** 4447–59
- [6] Turner M M and Hopkins M B 1992 *Phys. Rev. Lett.* **69** 3511–4
- [7] Vender D and Boswell R W 1992 *J. Vac. Sci. Technol. A* **10** 1331–8
- [8] Czarnetzki U, Luggenhölscher D and Döbele H F 1999 *Plasma Sources Sci. Technol.* **8** 230–48
- [9] Mussenbrock T, Brinkmann R P, Lieberman M A, Lichtenberg A J and Kawamura E 2008 *Phys. Rev. Lett.* **101** 085004
- [10] Schulze J, Heil B G, Luggenhölscher D, Mussenbrock T, Brinkmann R P and Czarnetzki U 2008 *J. Phys. D: Appl. Phys.* **41** 042003
- [11] Schulze J, Donkó Z, Luggenhölscher D and Czarnetzki U 2009 *Plasma Sources Sci. Technol.* **18** 034011
- [12] Turner M M 2009 *J. Phys. D: Appl. Phys.* **42** 194008
- [13] Gans T, O'Connell D, von der Gathen V S and Waskoenig J 2010 *Plasma Sources Sci. Technol.* **19** 034010
- [14] Schulze J, Schüngel E, Donkó Z, Luggenhölscher D and Czarnetzki U 2010 *J. Phys. D: Appl. Phys.* **43** 124016
- [15] Schulze J, Schüngel E, Donkó Z and Czarnetzki U 2010 *Plasma Sources Sci. Technol.* **19** 045028
- [16] Braginsky O, Kovalev A, Lopachev D, Proshina O, Rakhimova T, Vasilieva A, Voloshin D and Zyryanov S 2011 *J. Phys. D: Appl. Phys.* **45** 015201
- [17] Schüngel E, Schulze J, Donkó Z and Czarnetzki U 2011 *Phys. Plasmas* **18** 013503
- [18] Schulze J, Derzsi A, Dittmann K, Hemke T, Meichsner J and Donkó Z 2011 *Phys. Rev. Lett.* **107** 275001
- [19] Hemke T, Eremin D, Mussenbrock T, Derzsi A, Donkó Z, Dittmann K, Meichsner J and Schulze J 2012 *Plasma Sources Sci. Technol.* **22** 015012
- [20] Derzsi A, Korolov I, Schüngel E, Donkó Z and Schulze J 2013 *Plasma Sources Sci. Technol.* **22** 065009
- [21] Schulze J, Donkó Z, Derzsi A, Korolov I and Schuengel E 2014 *Plasma Sources Sci. Technol.* **24** 015019
- [22] Liu Y-X, Schüngel E, Korolov I, Donkó Z, Wang Y-N and Schulze J 2016 *Phys. Rev. Lett.* **116** 255002
- [23] Wilczek S et al 2016 *Phys. Plasmas* **23** 063514
- [24] Derzsi A, Bruneau B, Gibson A R, Johnson E, O'Connell D, Gans T, Booth J-P and Donkó Z 2017 *Plasma Sources Sci. Technol.* **26** 034002
- [25] Liu Y-X, Korolov I, Schüngel E, Wang Y-N, Donkó Z and Schulze J 2017 *Plasma Sources Sci. Technol.* **26** 055024
- [26] Bischoff L et al 2018 *Plasma Sources Sci. Technol.* **27** 125009
- [27] Schulze J, Donkó Z, Lafleur T, Wilczek S and Brinkmann R P 2018 *Plasma Sources Sci. Technol.* **27** 055010

- [28] Bogdanova M, Lopaev D, Zyryanov S, Voloshin D and Rakhi-mova T 2019 *Plasma Sources Sci. Technol.* **28** 095017
- [29] Gudmundsson J T and Proto A 2019 *Plasma Sources Sci. Technol.* **28** 045012
- [30] Press A F, Goeckner M J and Overzet L J 2019 *J. Vac. Sci. Technol. B* **37** 062926
- [31] Wang L, Wen D-Q, Zhang Q-Z, Song Y-H, Zhang Y-R and Wang Y-N 2019 *Plasma Sources Sci. Technol.* **28** 055007
- [32] Donkó Z 2001 *Phys. Rev. E* **64** 026401
- [33] Radmilović-Radjenović M and Petrović Z L 2009 *Eur. Phys. J. D* **54** 445–9
- [34] Greb A, Niemi K, O’Connell D and Gans T 2013 *Appl. Phys. Lett.* **103** 244101
- [35] Lafleur T, Chabert P and Booth J P 2013 *J. Phys. D: Appl. Phys.* **46** 135201
- [36] Hannesdottir H and Gudmundsson J T 2016 *Plasma Sources Sci. Technol.* **25** 055002
- [37] Horváth B, Daksha M, Korolov I, Derzsi A and Schulze J 2017 *Plasma Sources Sci. Technol.* **26** 124001
- [38] Horváth B, Schulze J, Donkó Z and Derzsi A 2018 *J. Phys. D: Appl. Phys.* **51** 355204
- [39] Daksha M, Derzsi A, Mujahid Z, Schulenberg D, Berger B, Donkó Z and Schulze J 2019 *Plasma Sources Sci. Technol.* **28** 034002
- [40] Sun G-Y, Li H-W, Sun A-B, Li Y, Song B-P, Mu H-B, Li X-R and Zhang G-J 2019 *Plasma Processes Polym.* **16** 1900093
- [41] Sun J-Y, Wen D-Q, Zhang Q-Z, Liu Y-X and Wang Y-N 2019 *Phys. Plasmas* **26** 063505
- [42] Phelps A V and Petrovic Z L 1999 *Plasma Sources Sci. Technol.* **8** R21–44
- [43] Gans T, Schulz-von der Gathen V and Döbele H F 2004 *Contrib. Plasma Phys.* **44** 523–8
- [44] Hockney R W and Eastwood J W 1981 *Computer Simulation Using Particles* (New York: McGraw-Hill)
- [45] Birdsall C K and Langdon A B 1985 *Plasma Physics via Computer Simulation* (New York: McGraw-Hill)
- [46] Birdsall C K 1991 *IEEE Trans. Plasma Sci.* **19** 65–85
- [47] Schweigert V A, Alexandrov A L, Gimelshtein S F and Ivanov M S 1999 *Plasma Sources Sci. Technol.* **9** B1–3
- [48] Diomede P, Capitelli M and Longo S 2005 *Plasma Sources Sci. Technol.* **14** 459–66
- [49] Verboncoeur J P 2005 *Plasma Phys. Control. Fusion* **47** A231–60
- [50] Matyash K, Schneider R, Taccogna F, Hatayama A, Longo S, Capitelli M, Tskhakaya D and Bronold F 2007 *Contrib. Plasma Phys.* **47** 595–634
- [51] Donkó Z 2011 *Plasma Sources Sci. Technol.* **20** 024001
- [52] Donkó Z, Schulze J, Czarnetzki U, Derzsi A, Hartmann P, Korolov I and Schüngel E 2012 *Plasma Phys. Control. Fusion* **54** 124003
- [53] Gudmundsson J T, Kawamura E and Lieberman M A 2013 *Plasma Sources Sci. Technol.* **22** 035011
- [54] Sun A, Becker M M and Loffhagen D 2016 *Comput. Phys. Commun.* **206** 35–44
- [55] Daksha M, Berger B, Schuengel E, Korolov I, Derzsi A, Koepke M, Donkó Z and Schulze J 2016 *J. Phys. D: Appl. Phys.* **49** 234001
- [56] Liu G-H, Liu Y-X, Bai L-S, Zhao K and Wang Y-N 2018 *Phys. Plasmas* **25** 023515
- [57] Kramida A, Ralchenko Yu, Reader J and NIST ASD Team 2019 NIST Atomic Spectra Database (ver. 5.7.1) National Institute of Standards and Technology, Gaithersburg, MD. <https://doi.org/10.18434/T4W30F>
- [58] Biagi S F 2004 Biagi-v7.1 database www.lxcat.net (Accessed: 8 April 2019) Cross sections extracted from PROGRAM MAGBOLTZ, VERSION 7.1 JUNE 2004
- [59] Phelps A V ftp://jila.colorado.edu/collision_data/ unpublished, retrieved on August 22, 2005
- [60] Kollath R 1956 *Encyclopedia of Physics* vol 21 ed S Flügge (Berlin: Springer) p 264
- [61] Demidov V I, Adams S F, Kaganovich I D, Koepke M E and Kurlyandskaya I P 2015 *Phys. Plasmas* **22** 104501
- [62] Sun G-Y, Li Y, Zhang S, Song B-P, Mu H-B, Guo B-H, Sun A-B and Zhang G-J 2019 *Plasma Sources Sci. Technol.* **28** 055001
- [63] Brinkmann R P 2007 *J. Appl. Phys.* **102** 093303
- [64] Biagi S F 2011 Biagi database www.lxcat.net (Accessed: 18 February 2020) Transcribed from S F Biagi’s Fortran Magboltz, version 8.97 (Sept 2011)